Natural Resources Research, Vol. 30, No. 1, February 2021 (© 2020)
https://doi.org/10.1007/s11053-020-09723-2

Original Paper

Quantitative Analysis of Pore Structure and Its Impact on Methane Adsorption Capacity of Coal

Shipei Xu,[1,3] Erfeng Hu,[2,4] Xingchun Li,[1,4] and Yu Xu[1]

Received 28 May 2020; accepted 9 July 2020
Published online: 26 July 2020

Better understanding of the storage and transportation characteristics of methane in coal seams is important to further develop and utilize the methane resources in the coalbed. This study is devoted to investigating the relationship between methane adsorption performance and pore structure by analyzing twelve coal samples derived from the typical methane-rich coalbeds in China. To eliminate the influence of inorganic components such as ash in different coal samples, a specific fixed-bed reactor with internals was employed for the coal treatment. Based on N_2/CO_2 adsorption analysis at low-pressure condition, the pores in coal were classified into three types in this study: ultra-micropore (pore width < 1 nm), micropore (1 nm < pore width < 2 nm) and mesopores (2 nm < pore width < 50 nm). According to the Langmuir equation, the Langmuir volume (V_L) and Langmuir pressure (P_L) were calculated to characterize the high-pressure adsorption of methane, and the influence of methane adsorption associated parameters was evaluated. The results indicate that N_2-pore size distributions (1–50 nm) varied a lot among samples, suggesting the significant heterogeneity of pore structure among samples. Estimated by the FHH model, pore surface fractal dimension (D_1) and spatial geometry fractal dimension (D_2) were, respectively, ranging in 2.059–2.808 and 2.649–2.852, which indicated that the more irregular surface, namely more inhomogeneous pore structures, resulted in the more surface area and stronger adsorption capability. By grey relational analysis (GRA), the importance of the pore structure factors on methane adsorption was identified, as an order from the most important to the least: ultra-micropore volume (0.9085) > ultra-micropore surface area (0.8976) > fractal dimension D_1 (0.8862) > N_2-BET surface area (0.7915) > micropore volume (0.5035) > micropore surface area (0.5006). This study shows the influence of parameters of pore structure on methane adsorption of coal and clarifies the order importance of these parameters by the GRA method.

KEY WORDS: Methane adsorption, Pore structure, Modified coal, Fractal dimension, Grey relational analysis.

INTRODUCTION

Methane is the main component of coal bed methane (CBM), accounting for 95–98% of its volume. Its absorbability and flowability in CBM system are closely related to the pore structure of coal (Zhang et al. 2019b; Fan et al. 2020). Thus, it is of great significance to investigate the pore structure of

[1]State Key Laboratory of Petroleum Pollution Control, CNPC Research Institute of Safety and Environmental Technology, Beijing 102206, China.
[2]State Key Laboratory of Coal Mine Disaster Dynamics and Control, Chongqing University, Chongqing 400044, China.
[3]State Key Laboratory of Multi-phase Complex Systems, Institute of Process Engineering, Chinese Academy of Sciences, Beijing 100190, China.
[4]To whom correspondence should be addressed; e-mail: huerfeng@qq.com, lixingchun_cnpc@126.com

coal, which is related to methane adsorption capacity. Coal is found to be a natural polymeric material with anisotropic porous structures (Gorbaty et al. 1986; Liu et al. 2019). It is generally believed that pores in coal have a wide size distribution and formed an interconnected network (Everett 1972). The pore size distribution of coal usually includes micropores (pore width < 2 nm), mesopores (2 nm $<$ pore width < 50 nm) and macropores (pore width > 50 nm), according to the International Union of Pure and Applied Chemistry (IUPAC) classification standard (Everett 1972; Macuda et al. 2020).

Different methods with varied purposes and accuracies have been adopted to investigate the pore structure of coal, such as nuclear magnetic resonance spectroscopy (NMR) (Genty et al. 2007; Yao et al. 2014), small-angle X-ray scattering (SAXS) (Zhao et al. 2014), small-angle neutron scattering (SANS) (Mastalerz et al. 2012), high-resolution transmission electron microscopy (HRTEM) (Harris and Yust 1976), Mercury intrusion porosimetry (MIP) (Clarkson and Marc Bustin 1996; Zhang et al. 2019a) and N_2/CO_2 gas adsorption analyses (Nguyen and Bhatia 2007). Each of these widely used techniques detects only a specific aperture range, but they cannot be used independently to describe the overall porosity or pore size distribution of samples. Among all the techniques, N_2/CO_2 gas adsorption analyses have been used widely to describe pore size distribution (Okolo et al. 2015). Okolo et al. (2015) used CO_2 gas adsorption techniques combined with the Horvath–Kawazoe (H–K) method and could only detect pores within the range of 0.3–0.65 nm. Mastalerz et al. (2008, 2012) stated an upper limit of 0.85 nm. N_2 analysis was believed to be able to detect the pores in the range from 1.7 to 300 nm. CO_2 gas adsorption is capable of measuring ultrafine micropore, while N_2 adsorption can provide a deep insight into the mesopore size distribution (Mahajan 1991; Walker and Mahajan 1993). Previous studies showed that most ranges of pore size distributions can be described by combining these two techniques. The properties of micropore sizes in the range of 0.85–1.7 nm are unclear and need further study (Okolo et al. 2015).

Based on the study of coal structure, further studies provided useful information about pore structure and methane adsorption capacity with N_2 and CO_2 adsorption. Experimental evidence shows that micropores play a dominant role in the adsorption of methane by coal (Hao et al. 2013). Yao et al. (2008) found that higher fractal dimension D_1 correlated with surfaces with higher irregularity, which provided more adsorption sites for methane. Higher fractal dimension D_2 was accompanied by higher heterogeneity of pore structure and higher liquid/gas surface tension that reduced CH_4 adsorption capacity (Yao et al. 2008; Li et al. 2018). Cai et al. (2013) found that adsorption-pore (pore size < 100 nm) controlled gas adsorption/diffusion, while seepage-pore (pore size > 100 nm) had obvious effects on and gas flow in coal seam. However, few studies had focused on quantitative analysis of influence degree related to these parameters. Analyzing the methane adsorption associated with the pore parameters independently and qualitatively needs further systematic and quantitative mathematical comprehensive investigation.

In this work, an indirectly heated fixed-bed with internals was employed for the treatment of coal samples, which made the modified samples with the same ash composition but different pore structures. This new reactor has been devised to enhance the heat transfer and pyrolysis performance, significantly increasing the coal tar yield and the transformation of char morphology structure (Hu et al. 2017). Besides, we adopted grey relational analysis (GRA), which is a useful method to evaluate the influence of various parameters without knowing their complex relationships (Zuo et al. 2016). The GRA method has been applied widely in various fields such as engineering technology, medicine, agriculture, petroleum industry and biology. However, the application of the GRA method to methane adsorption has not been reported to our limited knowledge. Therefore, this work aimed to: (1) describe the full range of micro-/mesopore size distribution; (2) define the pore structure parameters associated with methane adsorption capacity by linear fitting; and (3) study the influence degree of structure parameters, and try to find the sequence of degrees by GRA method.

METHODOLOGY

Samples and Thermal Conversion Procedure

Six typical different coal samples with different coal ranks were collected from active underground coal seams in China. All samples were crushed into 40–80 mesh size particles and were sealed and evacuated at 80 °C for 24 h before heat treatment.

The heat treatment experiments adopted a fixed-bed reactor made of 304-type stainless steel (Fig. 1). The reactor was 400 mm in height and 30 mm in inner diameter. A screen plate was welded in the right middle of the reactor to support the coal samples. Above the screen plate, there were four metal plates attached to the wall of the reactor at the angles of 90° with their width of 10 mm, height of 100 mm and thickness of 3 mm. The reactor was electrically heated externally with its temperature controlled by a proportional integral and differential controller connecting with a thermocouple. Nitrogen was adopted as the carrier gas with a flow of 100 ml/min and purity of 99.99%. 30 g coal sample was added to the reactor and heated to the preset temperature under nitrogen atmosphere. Nitrogen flow was not terminated into the reactor until its temperature dropped to room temperature. Then, modified coal samples were named in the form of ''coal seam—treatment temperature (°C)—treatment time (hour)''. The proximate and ultimate analysis data are shown in Table 1, according to the ASTMD7582 method (Xu et al. 2018b, 2019).

N_2/CO_2 Adsorption Characterization

Nitrogen and CO_2 adsorption characterization was performed via a physisorption apparatus (Quantachrome autosorb-6b/3B). The adsorption curves of nitrogen were measured at − 196°C under relative pressures (the gas pressure/the saturated vapor pressure, P/P_0) ranging from 0.001 to 0.995. The adsorption curves of CO_2 were measured under 0 °C within the standard atmospheric pressure range (0–0.101325 MPa). All samples were dried under vacuum at 80 °C for 10 h prior to the adsorption tests (Jagiello et al. 2015). The parameters of the pore were calculated by means of density functional theory (DFT) and automatically by the software of the physisorption apparatus (Nie et al. 2015).

High-Pressure Adsorption

Adsorption isotherms of methane under high pressure (up to 16 MPa) were obtained by static volumetric adsorption method (MTT752-1997, China standard). Approximately 15 g of the sample was used for each measurement. The void volume of the sample tube was measured by helium at the test temperature and then degassed at 80 °C for 10 h under vacuum. The methane adsorption capacity was measured with its peak pressure approached 16 MPa. The adsorption isotherm was analyzed to obtain adsorption parameters with the Langmuir model as (Langmuir 1918):

$$V = \frac{V_L \mathrm{P}}{\mathrm{P}+P_L} \tag{1}$$

where V_L, the Langmuir volume, is the maximum adsorption capacity of the material, while P_L, the Langmuir pressure, is the corresponding adsorption pressure when the adsorption volume (V) reaches half of V_L.

Grey Rational Analysis Calculation

GRA was used to calculate and compare the influence degree of pore parameters. The adsorption capacity, V_L, was expressed as $V = \{x_{10}, x_{20},\ldots, x_{m0}\}$. The adsorption parameters schemes were expressed as $F = \{F_1, F_2,\ldots, F_n\}$. Factor i of the sample j was expressed as x_{ij}. Due to different dimensions and units, the numerical values of different factors varied significantly. The different factors were standardized and transformed to compare after dividing by the average of the series. The standardized treatment of different factors was calculated as:

$$r_{ij} = \frac{x_{ij} - \min(\mathrm{x_i})}{\max(x_i) - \min(x_i)} \tag{2}$$

$$V = \{x_{10}, x_{20}, \ldots, x_{m0}\} \overset{\text{Standardizedtreatment}}{\Rightarrow} R_0 = \{r_{10}, r_{20}, \ldots r_{m0}\} \tag{3}$$

$$F = \begin{bmatrix} x_{11} & x_{12} & \cdots & x_{1n} \\ x_{21} & x_{22} & \cdots & x_{2n} \\ \cdots & \cdots & \cdots & \cdots \\ x_{m1} & x_{m2} & \cdots & x_{mn} \end{bmatrix} \overset{\text{Standardizedtreatment}}{\Rightarrow} R_n = \begin{bmatrix} r_{11} & r_{12} & \cdots & r_{1n} \\ r_{21} & r_{22} & \cdots & r_{2n} \\ \cdots & \cdots & \cdots & \cdots \\ r_{m1} & r_{m2} & \cdots & r_{mn} \end{bmatrix} \tag{4}$$

After standardization, the evaluation factors were converted into $R_j = (r_{1j}, r_{2j},\ldots r_{mj})^T$, while the optimal factor was converted into $R_0 = (r_{10}, r_{20},\ldots r_{m0})$. The multidimensional grey relational coefficient was calculated as:

$$\xi_{ij} = \frac{\min_i \min_j |r_{i0} - r_{ij}| + \rho \max_i \max_j |r_{i0} - r_{ij}|}{|r_{i0} - r_{ij}| + \rho \max_i \max_j |r_{i0} - r_{ij}|} \tag{5}$$

where ρ was applied to prevent the effect of $\max_i |r_{i0} - r_{ij}|$ from becoming too large, thus controlling the amplifying effect of different relation

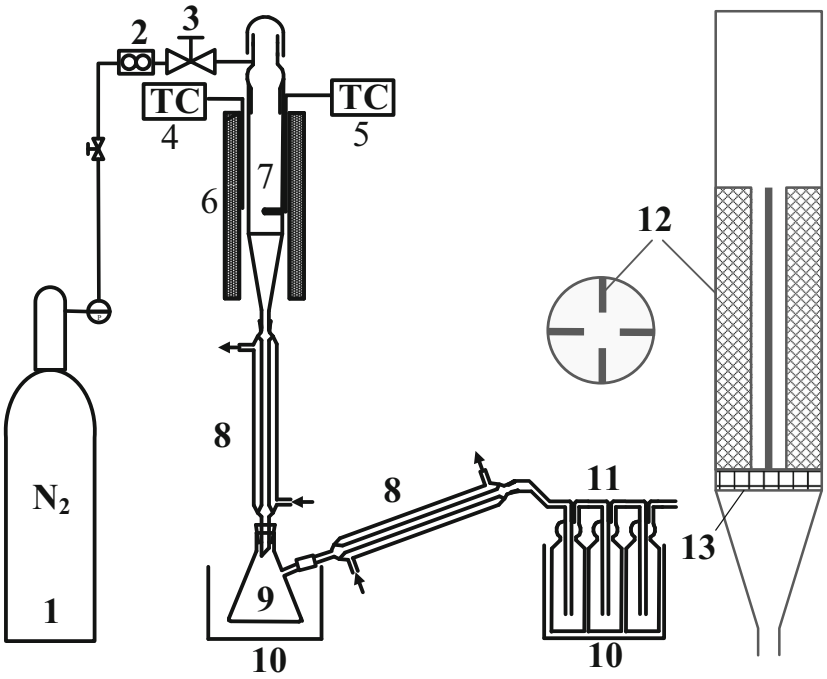

Figure 1. Schematic diagram of the experimental apparatus. (1) Nitrogen cylinder. (2) Mass flow controller. (3) Valve. (4) Furnace thermocouple. (5) Reactor thermocouple. (6) Furnace. (7) Quartz tube reactor. (8) Condenser. (9) Collection bottle. (10) Ice-water bath. (11) Acetone trap. (12) Metal plates. (13) Screen plate.

Table 1. Proximate and ultimate analyses of samples

Sample	Proximate analysis (wt.%, dry base)			Ultimate analysis (wt.%, daf base)				
	Volatile	Fixed carbon	Ash	C	H	N	S	O[a]
HN	31.48	46.03	22.48	81.55	5.57	1.38	0.61	10.88
HLJ	39.59	45.43	14.98	75.60	5.70	1.36	0.33	17.01
WYM	20.19	77.23	2.58	85.33	4.10	1.38	0.28	8.90
SX	31.17	60.30	8.53	78.90	4.37	0.98	0.32	15.43
XJ	44.19	43.92	11.89	73.35	5.73	1.04	0.45	19.43
SM	34.47	60.93	4.60	80.88	5.19	1.20	0.71	12.02
XJ-400-40	20.64	62.24	17.12	84.80	3.99	1.38	0.63	9.19
XJ-400-80	19.75	63.27	16.98	70.94	3.24	1.20	1.07	23.56
SM-300-40	32.19	62.79	5.03	82.34	4.94	1.24	0.26	11.22
SM-300-80	31.37	63.43	5.20	82.80	4.86	1.28	0.28	10.78
SM-400-40	15.39	78.57	6.03	86.48	3.89	1.42	0.31	7.91
SM-400-80	16.44	77.46	6.10	86.71	3.56	1.45	0.26	8.02

[a]By difference

coefficient. In this study, ρ was set to 0.5, the recommended value, which ensured both moderate distinguishing effects and good stability of outcomes (Nelabhotla et al. 2016).

The multidimensional grey relational matrix U was calculated from the matrix R_n (m factors of n samples) and Eq. (5), thus:

$$U = \begin{bmatrix} \xi_{11} & \xi_{12} & \cdots & \xi_{1n} \\ \xi_{21} & \xi_{22} & \cdots & \xi_{2n} \\ \cdots & \cdots & \cdots & \cdots \\ \xi_{m1} & \xi_{m2} & \cdots & \xi_{mn} \end{bmatrix} \quad (6)$$

Finally, grey relational grade (γ_i) was calculated as:

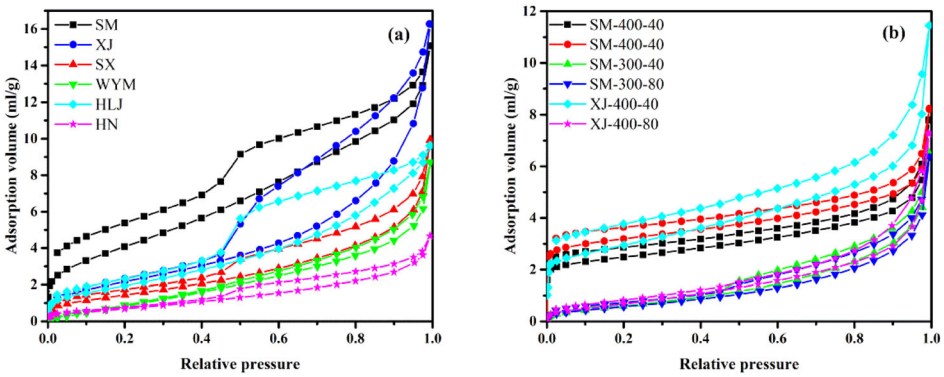

Figure 2. N_2 adsorption–desorption isotherms of samples: (**a**) coal; (**b**) modified coal.

$$\gamma_i = \frac{1}{n}\sum \xi_{ij} \tag{7}$$

RESULTS AND DISCUSSION

Quantitative Analyses of Pore Structure

Nitrogen adsorption analysis is used widely to characterize pore distribution in coal. Figure 2 demonstrates that the adsorption lines vary between different coal and modified coal with different treatments. The hysteresis lines of samples belong to H3 type according to IUPAC, because of capillary condensation of slit-shaped mesopores (Thommes 2010). Isotherm hysteresis still occurred at low relative pressures indicating the existence of intercalation, a solid swelling because of layered structures in materials (Cai et al. 2013; Xu et al. 2018a). The low-rank coals have more obvious adsorption hysteresis effect compared with high-rank anthracite (WYM), indicating that mesopores collapse during coalification. Similar results can be found between raw coal and modified coal after heat treatment of SM and XJ. Coalification has some similarity with heat treatment, especially the heat treatment under low temperature for a longtime (Landais 1991; Behar and Hatcher 1995). Generally, diagenesis has transformed organic matter at higher thermal maturity, generating more microporosity and reducing heterogeneity of pore surface (Levy et al. 1997). This process often occurred in high-rank coal with high adsorption capacity (Bustin and Clarkson 1998). Therefore, the SM, XJ raw coals and modified coals can be regarded as a series of coals with varied coalification degrees. Moreover, it reduces the influence of inorganic matter when comparing the influence of pore characterization on methane adsorption.

The pore parameters estimated with N_2 adsorption are listed in Table 2. Sample SM-400-80 has the smallest average pore size but has the largest BET surface area. Sample XJ has the largest average pore size and the largest BJH mesopores volume. The results indicate that pores with smaller size contribute more to surface area, while those with larger size dominate over pore volume (Wang et al. 2016).

Density functional theory (DFT) and molecular simulation can be adopted to analyze accurately the pore size distribution (PSD) over the complete micropore–mesopore size range within a single method (Thommes 2010). The DFT-PSDs of all samples are shown in Figure 3, which can be divided into four categories according to their distinctions. Category I has the most intensive peak below 2 nm and dispersive peaks above 2 nm, including XJ-400-40, SM-400-40 and SM-400-80. Category II has intensity peak below 2 nm and intensive peaks in the range above 2 nm, including SX and SM. Categories III and IV have little or no peak below 2 nm. Category III has dispersive peaks above 2 nm, including WYM, XJ-400-80, SM-300-40 and SM-300-80, while category IV has intensive peaks above 2 nm, including HN, HLJ and XJ. These pore size distributions in different categories influenced the fractal analysis of samples as discussed below.

It is hard to analyze ultrafine pores with nitrogen due to its low diffusion rate under low temperature. However, CO_2 is recognized as a good alternative, primarily because of higher operating temperatures (usually 0 °C) (De Jonge and Mittelmeijer-Hazeleger 1996). Figure 4 shows the CO_2

Table 2. Structural pore parameters of samples

Sample ID	V_L (ml/g)	P_L (MPa)	N_2 adsorption			CO_2 adsorption		
			N_2 BJH pore volume ($\times 10^{-3}$ ml/g)	N_2 BET surfaces area (m^2/g)	Average pore size (nm)	CO_2 DFT pore volume ($\times 10^{-3}$ ml/g)	CO_2 DFT surface area (m^2/g)	Average pore size (nm)
HN	13.96	30.45	7	3.14	9.21	23	64.26	0.6
HLJ	24.62	26.95	16	7.78	7.64	51	147.53	0.5
WYM	28.16	21.32	13	5.47	10.26	71	231.96	0.48
SX	31.40	29.55	15	5.66	10.87	65	209.53	0.57
XJ	25.14	36.76	28	8.37	12.03	60	182.48	0.48
SM	29.88	19.72	19	5.43	6.04	61	193.82	0.5
XJ-400-40	37.46	24.31	13	10.34	6.85	81	269.3	0.46
XJ-400-80	28.40	11.41	11	3.11	5	81	276.13	0.48
SM-300-40	23.87	16.22	11	2.78	4.56	47	153.10	0.50
SM-300-80	26.26	19.80	10	2.46	6.11	61	188.66	0.48
SM-400-40	30.64	13.09	8	9.1	5.31	68	223.61	0.51
SM-400-80	42.34	18.11	8	11.91	4.26	80	270.14	0.5

adsorption isotherms. It can be confirmed that all samples are microporous materials owning to their Type I isotherms.

Both CO_2-DFT pore volume and surface area are listed in Table 2. The DFT-PSDs of 12 samples show their major peaks ranging from 0.35 to 1 nm (Fig. 5). There were no pores above 1 nm because of the high test temperature (0 °C). The higher the temperature is, the larger the fugacity of CO_2 molecule gets, and the higher the adsorption equilibrium pressure becomes. However, the maximum analysis pressure was standard atmospheric pressure. In this condition, CO_2 can only be used to analyze pores less than 1 nm.

Fractal geometry is a powerful method for the quantitative study of pore structure and surface irregularity that directly affects pore adsorption and diffusion behavior. The FHH model had the high universality of many rock types, including coals. All FHH plots are displayed in Figure 6. Each picture had two obvious straight fitting-lines in the P/P_0 ranges below and above 0.5. The coefficients of determination of all fitting-lines were higher than 0.92 (Table 3). The results indicate that there are two different adsorption mechanisms of the tested coal samples.

Methane Adsorption Capacity

Figure 7 displays the isotherms of excess methane adsorption measured by the volumetric method. Based on IUPAC classification, all the isotherms belong to Type I (Fig. 7), indicating that the Langmuir adsorption mode is suitable to analyze them quantitatively. All calculated results are shown in Table 2. The adsorption capacities of the samples were in the ranges of 11.27–27.06 and 21.36–39.26 ml/g, respectively.

Influence of Fractal Dimensions on Methane Adsorption

Methane adsorption character varies with not only temperature and pressure but also the physical properties of adsorbent (Yang and Saunders 1985). Among several physical properties, few attempts have been made on the effects of the fractal characteristics of coal pores on methane adsorption (Liu and Nie 2016). Each sample had two fractal dimensions, D_1 and D_2, which had different impacts on methane adsorption.

D_1 was calculated using the data with P/P_0 of ≤ 0.5. The van der Waals forces between adsorbate and surface of adsorbent dominate the adsorption process, resulting in monolayer adsorption on the surface. Consequently, D_1 reflects the surface roughness of the pore structure. D_2 was calculated using the data with P/P_0 of > 0.5. The adsorption mechanism transits from monolayer adsorption with P/P_0 of ≤ 0.5 to multidimensional and pore-filling adsorption with P/P_0 of > 0.5. Therefore, D_2 can be used to define the irregularity of pore structure (Yao et al. 2008; Sun et al. 2015). It is interesting to find that samples with N_2-PSD of category I (XJ-400-40,

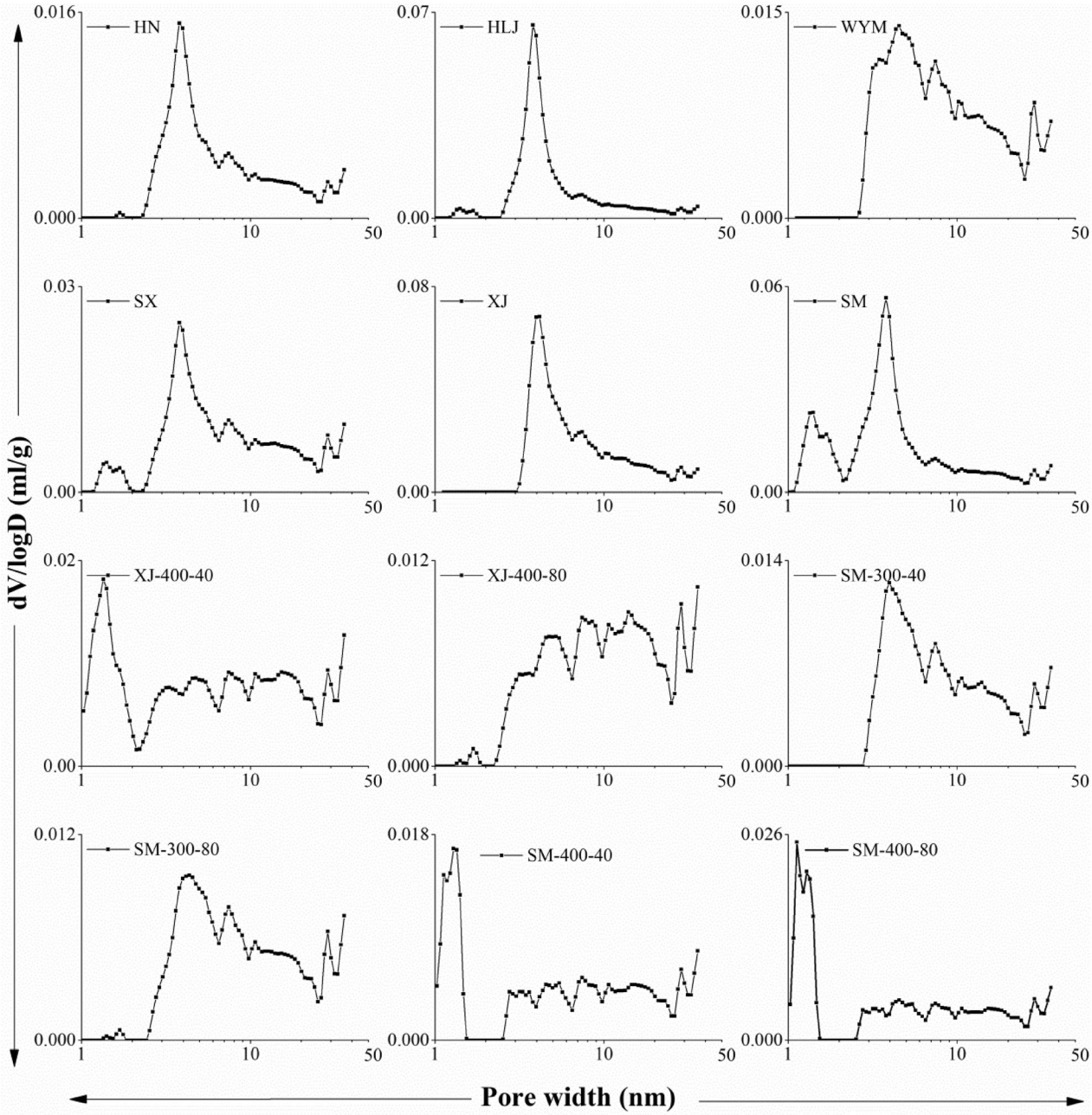

Figure 3. DFT-PSDs obtained from N_2 adsorption isotherms.

SM-400-40 and SM-400-80) have larger D_1 than the others. It could be comprehended that the surface of material with micropore and disorder mesopores is rougher than that with uniform pores.

The two fractal dimensions, D_1 and D_2, have significantly different effects on V_L and P_L of samples (Fig. 8). V_L has a positive liner relationship with D_1 because rougher surface adsorbents with higher values of D_1 have more active sites for methane adsorption (Wang et al. 2016). However, similar to previous reports (Cai et al. 2013; Wang et al. 2016), there is no obvious relationship between D_2 and V_L,

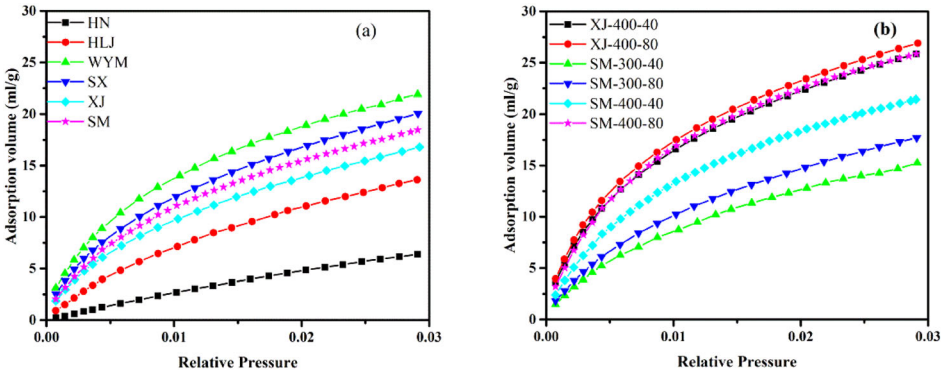

Figure 4. CO_2 adsorption–desorption isotherms of samples: (**a**) coal; (**b**) modified coal.

or between D_1/D_2 and P_L. It is deduced that adsorbents with higher D_1 have more micropores and more irregular and rougher coal surfaces, which can offer more sites for methane adsorption, resulting in their higher V_L values.

Influence of Pore Structures on Methane Adsorption

The adsorption capacity of coal samples is associated closely with micro-/mesopore characteristics. Therefore, it is of great significance to analyze the full range micro-/mesopore size distribution (0.3–50 nm). We quantified the full range micro-/mesopore (0.3–50 nm) by combining the N_2/CO_2 adsorption results (Figs. 3 and 5).

Figure 9 shows the relationship of pore structures and methane adsorption. Methane adsorption capacity is positively related to pore volume and surface area of pores with pore diameter less than 2 nm (0.3–1 nm from CO_2 data, 1–2 nm from N_2 data). However, in correspondence with previous results (Liu and He 2017), mesopore (2–50 nm) did not significantly influence methane adsorption (Fig. 9a, b and e). A linear relation can be found between BET surface area and V_L mainly because the former is dominated by micropore (Thommes 2010).

P_L shows a linear increase with the increase in average mesopores size (Fig. 10a). The reason for this phenomenon might be that the interaction energy between adsorbent and adsorbate in the center of pore decreases with rising pore size (Thommes 2010). Thus, the larger the pore size is, the larger the fugacity of methane molecule gets; consequently, the higher the adsorption equilibrium pressure becomes.

Grey Relational Analysis of Influence Factors

As discussed above, methane adsorption is a complex process influenced by several factors such as the fractal dimension D_1, micropore volume, micropore surface area, N_2 BET surface area, ultramicropore volume and ultra-micropore surface area. In order to analyze the influence degree of different factors on adsorption performance, the GRA method was adopted. Based on the GRA method and the above experimental data, the reference and comparison sequences were first constructed as follows.

The reference sequence was:

$$V = \{13.96, 24.62, 28.16, 31.40, 25.14, 29.88, 37.46, 28.40, 23.87, 26.26, 30.64, 42.34\}^T$$

The reference sequence after standardized treatment was:

$$R_0 = \{0.49, 0.86, 0.99, 1.10, 0.88, 1.05, 1.31, 1.00, 0.84, 0.92, 1.07, 1.49\}^T$$

The comparison sequence was:

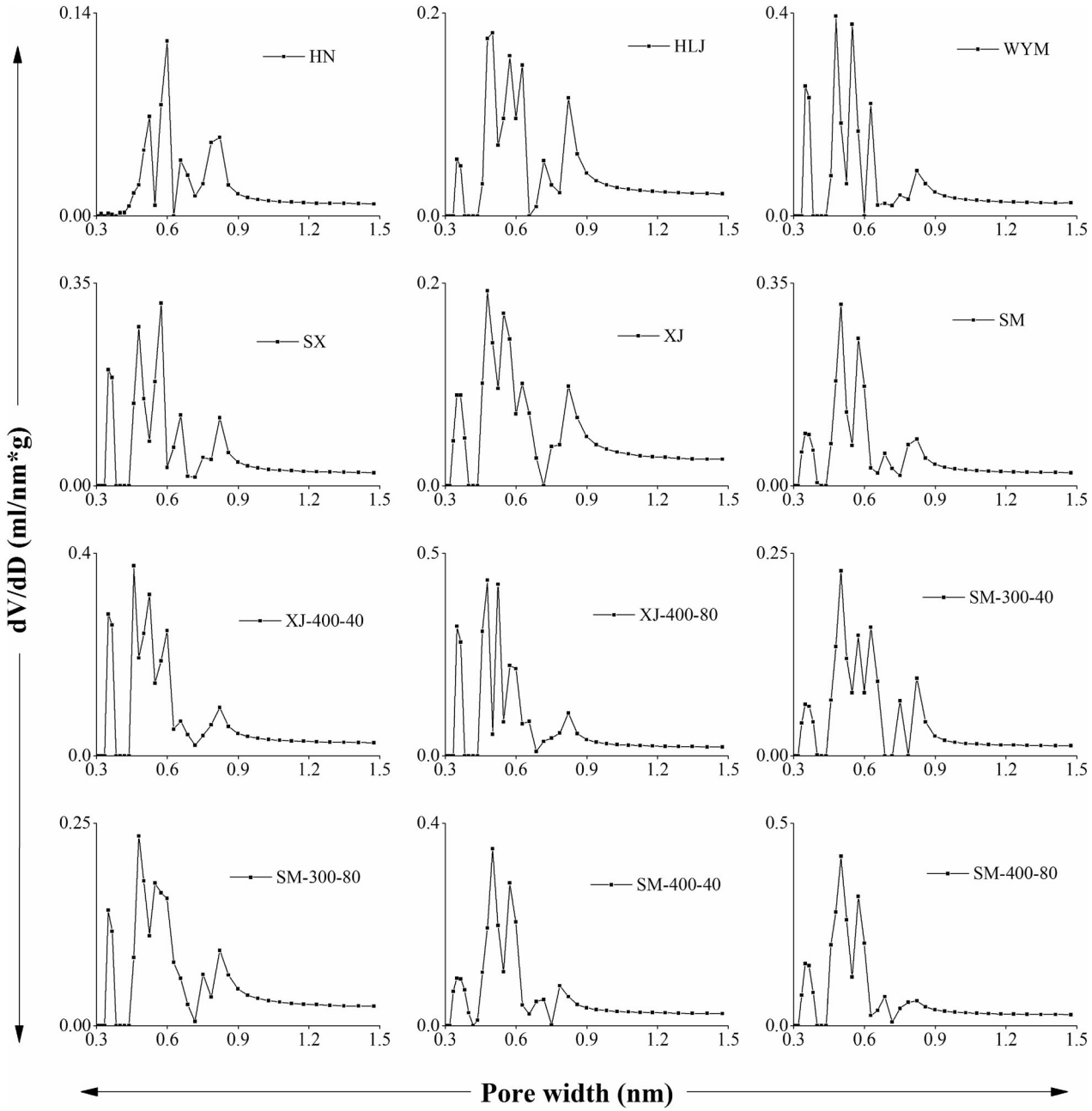

Figure 5. DFT-PSDs obtained from CO_2 adsorption isotherms.

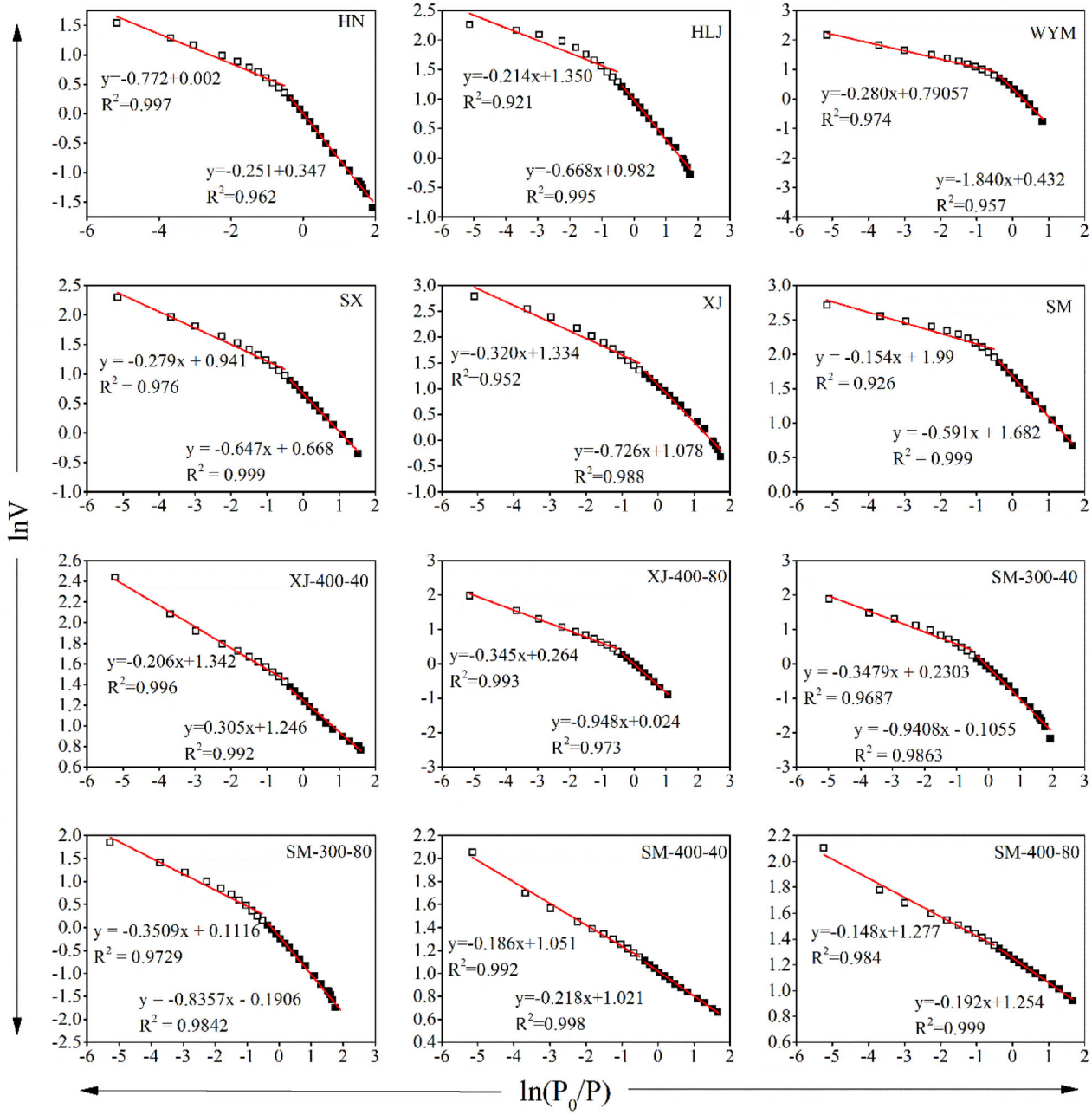

Figure 6. Plots of ln(V) vs. ln(ln(P_0/P)) reconstructed from N_2 adsorption isotherms.

Table 3. Fractal dimensions of samples

Sample ID	P/P_0: 0-0.5			P/P_0: 0.5-1		
	K_1	$D_1 = 3+K_1$	R^2	K_2	$D_2 = 3+K_2$	R^2
HN	− 0.772	2.228	0.997	− 0.251	2.749	0.962
HLJ	− 0.668	2.332	0.995	− 0.214	2.786	0.921
WYM	− 0.640	2.360	0.957	− 0.280	2.720	0.974
SX	− 0.647	2.353	0.999	− 0.279	2.721	0.976
XJ	− 0.726	2.274	0.988	− 0.320	2.680	0.952
SM	− 0.591	2.409	0.999	− 0.154	2.846	0.926
XJ-400-40	− 0.305	2.695	0.992	− 0.206	2.794	0.996
XJ-400-80	− 0.548	2.452	0.973	− 0.345	2.655	0.993
SM-300-40	− 0.941	2.059	0.986	− 0.348	2.652	0.969
SM-300-80	− 0.836	2.164	0.948	− 0.351	2.649	0.973
SM-400-40	− 0.218	2.782	0.998	− 0.186	2.814	0.992
SM-400-80	− 0.192	2.808	0.999	− 0.148	2.852	0.984

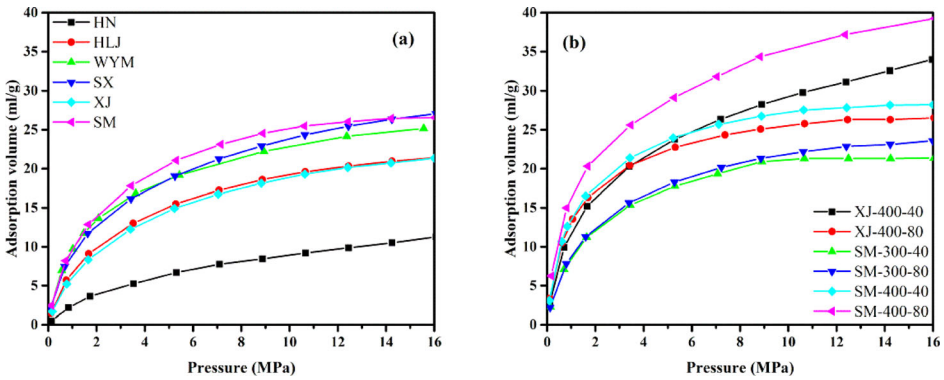

Figure 7. Methane excess adsorption isotherms of samples: (**a**) coals; (**b**) modified coals.

$$F = \begin{bmatrix} 2.228 & 3.14 & 0.018 & 0.016 & 64 & 23 \\ 2.332 & 7.78 & 0.458 & 0.349 & 148 & 51 \\ 2.360 & 5.47 & 0.000 & 0.000 & 232 & 71 \\ 2.353 & 5.66 & 0.789 & 0.606 & 210 & 65 \\ 2.274 & 8.37 & 0.000 & 0.000 & 182 & 60 \\ 2.409 & 5.43 & 5.093 & 3.853 & 194 & 61 \\ 2.695 & 10.34 & 6.596 & 3.994 & 269 & 81 \\ 2.452 & 3.11 & 0.081 & 0.067 & 276 & 81 \\ 2.059 & 2.78 & 0.000 & 0.000 & 153 & 47 \\ 2.164 & 2.46 & 0.044 & 0.036 & 189 & 61 \\ 2.782 & 9.10 & 7.101 & 3.433 & 224 & 68 \\ 2.808 & 11.91 & 9.488 & 4.606 & 270 & 80 \end{bmatrix}$$

The comparison sequence after standardized treatment was:

$$R_n = \begin{bmatrix} 0.92 & 0.50 & 0.01 & 0.01 & 0.32 & 0.37 \\ 0.97 & 1.24 & 0.19 & 0.25 & 0.73 & 0.82 \\ 0.98 & 0.87 & 0.00 & 0.00 & 1.15 & 1.14 \\ 0.98 & 0.90 & 0.32 & 0.43 & 1.04 & 1.04 \\ 0.94 & 1.33 & 0.00 & 0.00 & 0.91 & 0.96 \\ 1.00 & 0.86 & 2.06 & 2.73 & 0.96 & 0.98 \\ 1.12 & 1.64 & 2.67 & 2.83 & 1.34 & 1.30 \\ 1.02 & 0.49 & 0.03 & 0.05 & 1.37 & 1.30 \\ 0.85 & 0.44 & 0.00 & 0.00 & 0.76 & 0.75 \\ 0.90 & 0.39 & 0.02 & 0.00 & 0.94 & 0.98 \\ 1.15 & 1.45 & 2.87 & 2.43 & 1.11 & 1.09 \\ 1.17 & 1.89 & 3.84 & 3.27 & 1.34 & 1.28 \end{bmatrix}$$

The multidimensional grey relational matrix U was calculated by the matrix R_n, thus:

$$U = \begin{bmatrix} 0.7352 & 0.9994 & 0.7142 & 0.7158 & 0.8800 & 0.9130 \\ 0.9251 & 0.7648 & 0.6387 & 0.6610 & 0.9074 & 0.9687 \\ 1.0000 & 0.9151 & 0.5474 & 0.5474 & 0.8818 & 0.8932 \\ 0.9103 & 0.8595 & 0.6048 & 0.6410 & 0.9594 & 0.9581 \\ 0.9567 & 0.7296 & 0.5756 & 0.5756 & 0.9847 & 0.9433 \\ 0.9674 & 0.8700 & 0.5413 & 0.4141 & 0.9406 & 0.9500 \\ 0.8635 & 0.7869 & 0.4681 & 0.4396 & 0.9846 & 0.9934 \\ 0.9889 & 0.7057 & 0.5536 & 0.5575 & 0.7618 & 0.8014 \\ 0.9923 & 0.7533 & 0.5883 & 0.5883 & 0.9467 & 0.9398 \\ 0.9879 & 0.6940 & 0.5697 & 0.5648 & 0.9916 & 0.9610 \\ 0.9431 & 0.7659 & 0.3984 & 0.4672 & 0.9752 & 0.9946 \\ 0.7917 & 0.7485 & 0.3357 & 0.4006 & 0.8996 & 0.8585 \end{bmatrix}$$

Finally, from the coefficient matrix [U], the grey relational grades between coal structure parameters and the methane adsorption capacity were calculated, thus: $\gamma_1 = 0.9218$ (D_1), $\gamma_2 = 0.7994$ (N_2 BET surfaces area), $\gamma_3 = 0.5446$ (micropore surface area), $\gamma_4 = 0.5486$ (micropore volume), $\gamma_5 = 0.9261$ (ultra-micropore surface area) and $\gamma_6 = 0.9312$ (ultra-micropore volume). In conclusion, the order of influence degree of coal structure parameters on methane adsorption capacity was $\gamma_6 > \gamma_5 > \gamma_1 > {}_6 > \gamma_5 > \gamma_1 > \gamma_2 > \gamma_4 > \gamma_3$.

In the GRA, grey relational grade (γ_i) is correlated to the performance of different factors in a complex process. The higher γ_i one factor achieves, the more important it performs in such a process (Xu et al. 2011). The six influence factors of the methane adsorption process are listed by their performances as follows: ultra-micropore volume > ultra-micropore surface area > D_1 > N_2 BET surfaces area > micropore volume > micropore surface area. Generally, the grey relational grade represents different influence degree of varied factors, with $\gamma_i >$ 0.9, $\gamma_i > 0.8$, $\gamma_i > 0.7$, $\gamma i < 0.6$ representing marked influence, relatively marked influence, noticeable influence, and negligible influence, respectively. Ultra-micropore has stronger influence on methane adsorption capacity than micropore (Shen et al. 2015). Besides, ultra-micropore contains a large proportion of micropores whose pore size is believed to be the optimum dimension for methane adsorption, around 0.8 nm (Matranga et al. 1992). The grey relational grade of the pore volume is always higher than that of surface area, not only for micropores but also for ultra-micropores. Because of high-pressure adsorption, there was a solid swelling phenomenon in the coal sample, which increases the methane adsorption capacity of the sample. This phenomenon was more closely related to the pore volume than surface area. Therefore, compared with surface area, pore volume is a more important factor in gas sorption of coal, which is consistent with previous studies (Mastalerz et al. 2004; Clarkson et al. 2013; Hao et al. 2013).

Figure 9. Plots of pore structure parameters vs. Langmuir volume (V_L) of samples: (**a**) pore volume of pores in different size ranges; (**b**) surface area of pores in different size ranges; (**c**) ultra-micropore volume; (**d**) ultra-micropore surface area; (**e**) N_2 BJH mesopore volume; (f) N_2 BET surface area. ▶

CONCLUSIONS

The pore structure of all samples was characterized by N_2/CO_2 adsorption, and their high-pressure methane adsorption capacity was measured. By means of linear fitting, several coal structure parameters were found to influence methane adsorption capacity. Furthermore, the influence degree afforded by different structure parameters was

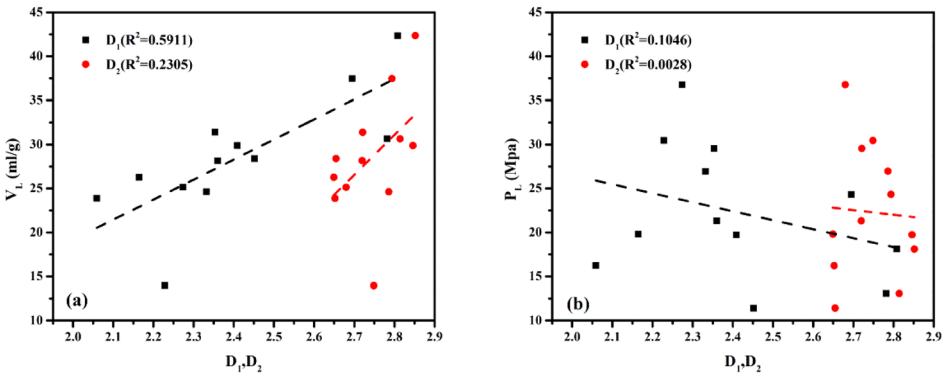

Figure 8. Influence of fractal dimensions on: (**a**) V_L; (**b**) P_L.

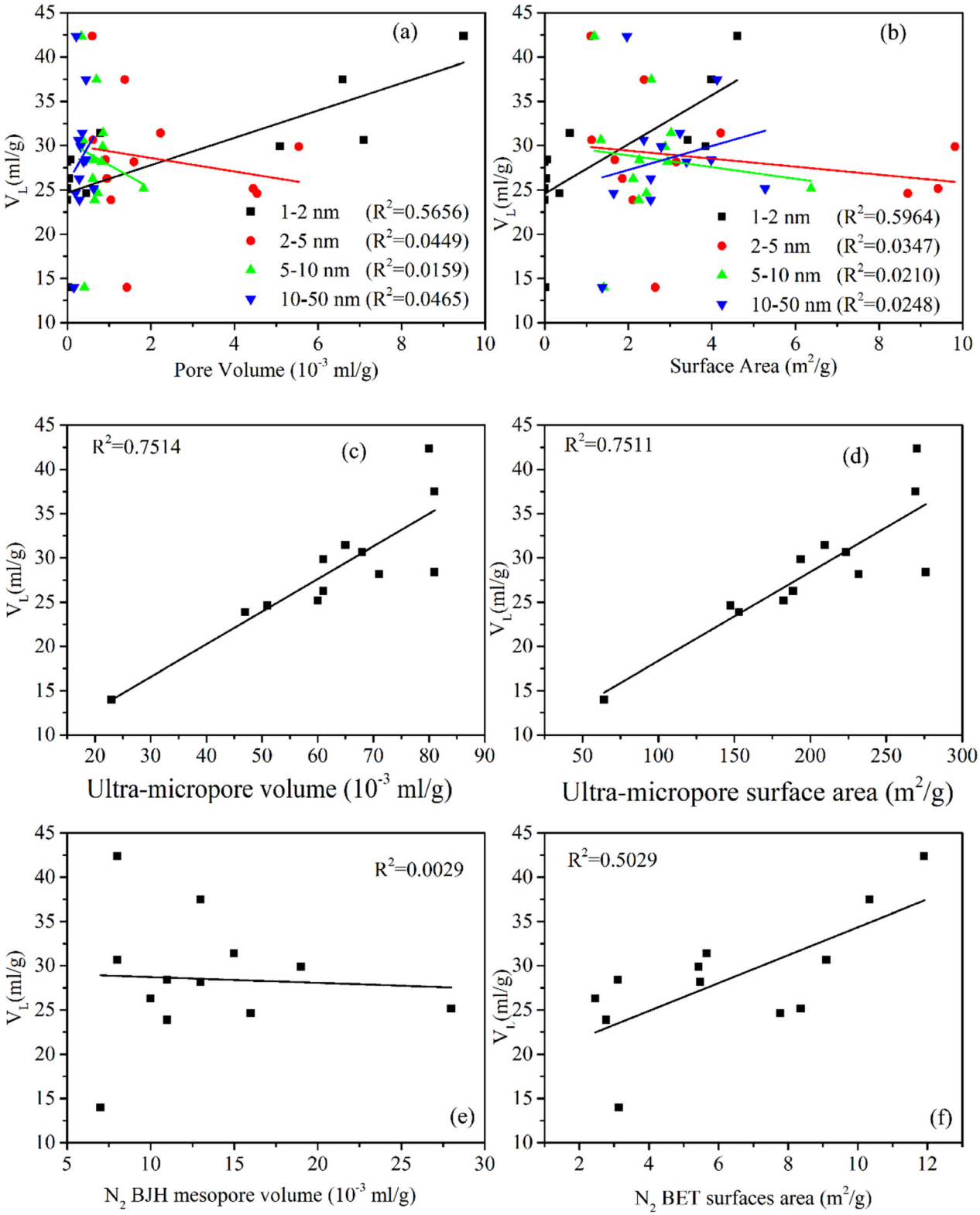
(a)
1-2 nm (R^2=0.5656)
2-5 nm (R^2=0.0449)
5-10 nm (R^2=0.0159)
10-50 nm (R^2=0.0465)
V_L (ml/g)
Pore Volume (10^{-3} ml/g)
(b)
1-2 nm (R^2=0.5964)
2-5 nm (R^2=0.0347)
5-10 nm (R^2=0.0210)
10-50 nm (R^2=0.0248)
V_L (ml/g)
Surface Area (m^2/g)
R^2=0.7514
(c)
V_L (ml/g)
Ultra-micropore volume (10^{-3} ml/g)
R^2=0.7511
(d)
V_L (ml/g)
Ultra-micropore surface area (m^2/g)
R^2=0.0029
(e)
V_L (ml/g)
N_2 BJH mesopore volume (10^{-3} ml/g)
R^2=0.5029
(f)
V_L (ml/g)
N_2 BET surfaces area (m^2/g)

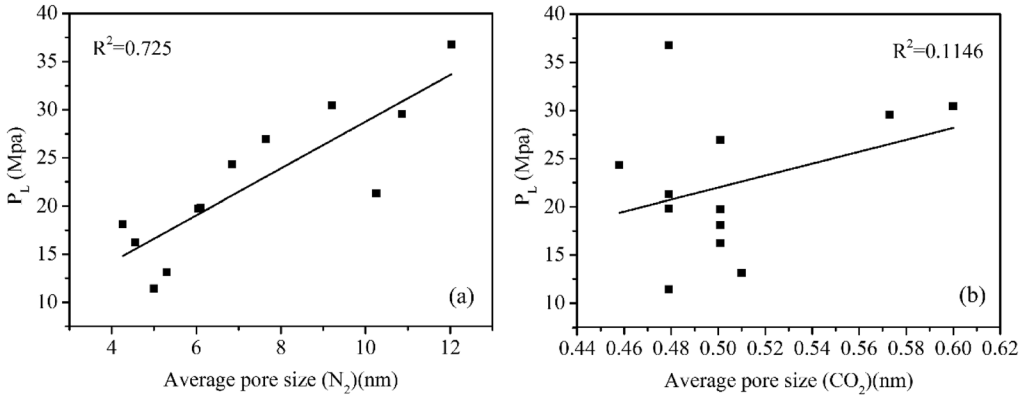

Figure 10. Plots of average pore size vs. Langmuir pressure (P_L) of samples: (**a**) from N_2 results; (**b**) from CO_2 results.

evaluated by GRA method. The major conclusions of this study are as follows:

(1) A full range micro-/mesopore size distribution was characterized by combining CO_2 and N_2 adsorption (0.3–1 nm by CO_2 adsorption and 1–50 nm by N_2 adsorption). Comprehensively analyzed from the pore structure and methane adsorption data, it could be found that both surface area and volume of pore with its width below 2 nm had significant influence on Langmuir volume (V_L), while average mesopore size is closely related to Langmuir pressure (P_L).
(2) Four categories PSDs were observed for all the samples. Category I, which had most intensive peak during 1–2 nm and dispersive peaks during 2–50 nm, had obviously larger D_1 than the other samples.
(3) Based on the N_2 adsorption data, two different fractal dimensions, D_1 and D_2, were obtained. D_1 ranged from 2.059 to 2.808, and D_2 ranged from 2.649 to 2.852. The higher pore surface fractal dimension (D_1) represented rougher surface, on which more active adsorption sites were available for methane, whereas D_2 did not influence the gas storage capacity.
(4) The grey relational grades of six factors (fractal dimension D_1, micropore volume, micropore surface area, N_2 BET surface area, ultra-micropore volume and ultra-micropore surface area) were 0.8862, 0.5035, 0.5006, 0.7915, 0.9085 and 0.8976, respectively. Therefore, the influence of the six factors were ranked by the importance from the most to the least as ultra-micropore volume, ultra-micropore surface area, fractal dimension D_1, N_2 BET surface area, micropore volume and micropore surface area. This study showed that GRA is a promising statistical method that can be used successfully for comparing influence of different pore parameters on methane adsorption.

ACKNOWLEDGMENTS

The study was financially supported by National Science and Technology Major Project of China (2016ZX05040-003). We thank Doctor Nie Fan for his linguistic assistance during the revise of this manuscript.

REFERENCES

Behar, F., & Hatcher, P. G. (1995). Artificial coalification of a fossil wood from brown coal by confined system pyrolysis. *Energy & Fuels, 9*(6), 984–994.

Bustin, R. M., & Clarkson, C. R. (1998). Geological controls on coalbed methane reservoir capacity and gas content. *International Journal of Coal Geology, 38*(1–2), 3–26.

Cai, Y., Liu, D., Pan, Z., Yao, Y., Li, J., & Qiu, Y. (2013). Pore structure and its impact on CH_4 adsorption capacity and flow capability of bituminous and subbituminous coals from Northeast China. *Fuel, 103,* 258–268.

Clarkson, C. R., & Marc Bustin, R. (1996). Variation in micropore capacity and size distribution with composition in bituminous coal of the Western Canadian Sedimentary Basin. *Fuel, 75*(13), 1483–1498.

Clarkson, C. R., Solano, N., Bustin, R. M., Bustin, A. M. M., Chalmers, G. R. L., He, L., et al. (2013). Pore structure characterization of North American shale gas reservoirs using USANS/SANS, gas adsorption, and mercury intrusion. *Fuel, 103,* 606–616.

De Jonge, H., & Mittelmeijer-Hazeleger, M. C. (1996). Adsorption of CO_2 and N_2 on Soil Organic Matter: Nature of Porosity, Surface Area, and Diffusion Mechanisms. *Environmental Science and Technology, 30*(2), 408–413.

Everett, D. H. (1972). Manual of symbols and terminology for physicochemical quantities and units, appendix II: definitions, terminology and symbols in colloid and surface chemistry. *Pure and Applied Chemistry, 31*(4), 577–638.

Fan, J., Liu, P., Li, J., & Jiang, D. (2020). A coupled methane/air flow model for coal gas drainage: model development and finite-difference solution. *Process Safety and Environmental Protection, 141,* 288–304.

Genty, C., Jensen, J. L., & Ahr, W. M. (2007). Distinguishing carbonate reservoir pore facies with nuclear magnetic resonance measurements. *Natural Resources Research, 16*(1), 45–54.

Gorbaty, M. L., Mraw, S. C., Gethner, J. S., & Brenner, D. (1986). Coal physical structure: porous rock and macromolecular network. *Fuel Processing Technology, 12,* 31–49.

Hao, S., Wen, J., Yu, X., & Chu, W. (2013). Effect of the surface oxygen groups on methane adsorption on coals. *Applied Surface Science, 264,* 433–442.

Harris, L., & Yust, C. (1976). Transmission electron microscope observations of porosity in coal. *Fuel, 55*(3), 233–236.

Hu, E., Zeng, X., Wang, F., Li, Y., Yi, X., & Fu, X. (2017). Effects of metallic heating plates on coal pyrolysis behavior in a fixed-bed reactor enhanced with internals. *Energy & Fuels, 31*(3), 2716–2721.

Jagiello, J., Ania, C., Parra, J. B., & Cook, C. (2015). Dual gas analysis of microporous carbons using 2D-NLDFT heterogeneous surface model and combined adsorption data of N_2 and CO_2. *Carbon, 91,* 330–337.

Landais, P. (1991). Assessment of coal potential evolution by experimental simulation of natural coalification. *Organic Geochemistry, 17*(6), 705–710.

Langmuir, I. (1918). The adsorption of gases on plane surfaces of glass, mica and platinum. *Journal of the American Chemical Society, 40*(9), 1361–1403.

Levy, J. H., Day, S. J., & Killingley, J. S. (1997). Methane capacities of Bowen Basin coals related to coal properties. *Fuel, 76*(9), 813–819.

Li, X., Li, Z., Wang, E., Liang, Y., Li, B., & Liu, Y. (2018). Pattern recognition of mine microseismic (MS) and blasting events based on wave fractal features. *Fractals, 26*(03), 1850029. https://doi.org/10.1142/s0218348x18500299.

Liu, X., & He, X. (2017). Effect of pore characteristics on coalbed methane adsorption in middle-high rank coals. *Adsorption, 23*(1), 3–12.

Liu, S., Li, X., Wang, D., Wu, M., Yin, G., & Li, M. (2019). Mechanical and acoustic emission characteristics of coal at temperature impact. *Natural Resources Research, 4,* 1–18.

Liu, X., & Nie, B. (2016). Fractal characteristics of coal samples utilizing image analysis and gas adsorption. *Fuel, 182,* 314–322.

Macuda, J., Baran, P., & Wagner, M. (2020). Evaluation of the presence of methane in złoczew lignite comparison with other lignite deposits in Poland. *Natural Resources Research*. https://doi.org/10.1007/s11053-020-09691-7.

Mahajan, O. P. (1991). CO_2 surface area of coals: The 25-year paradox. *Carbon, 29*(6), 735–742.

Mastalerz, M., Drobniak, A., & Rupp, J. (2008). Meso-and micropore characteristics of coal lithotypes: implications for CO_2 adsorption. *Energy & Fuels, 22*(6), 4049–4061.

Mastalerz, M., Gluskoter, H., & Rupp, J. (2004). Carbon dioxide and methane sorption in high volatile bituminous coals from Indiana, USA. *International Journal of Coal Geology, 60*(1), 43–55.

Mastalerz, M., He, L., Melnichenko, Y. B., & Rupp, J. A. (2012). Porosity of coal and shale: insights from gas adsorption and SANS/USANS techniques. *Energy & Fuels, 26*(8), 5109–5120.

Matranga, K. R., Myers, A. L., & Glandt, E. D. (1992). Storage of natural gas by adsorption on activated carbon. *Chemical Engineering Science, 47*(7), 1569–1579.

Nelabhotla, D. M., Jayaraman, T. V., Asghar, K., & Das, D. (2016). The optimization of chemical mechanical planarization process-parameters of c-plane gallium-nitride using Taguchi method and grey relational analysis. *Materials and Design, 104,* 392–403.

Nguyen, T. X., & Bhatia, S. K. (2007). Pore accessibility of N_2 and Ar in disordered nanoporous solids: theory and experiment. *Adsorption, 13*(3–4), 307–314.

Nie, B., Liu, X., Yang, L., Meng, J., & Li, X. (2015). Pore structure characterization of different rank coals using gas adsorption and scanning electron microscopy. *Fuel, 158,* 908–917.

Okolo, G. N., Everson, R. C., Neomagus, H. W. J. P., Roberts, M. J., & Sakurovs, R. (2015). Comparing the porosity and surface areas of coal as measured by gas adsorption, mercury intrusion and SAXS techniques. *Fuel, 141,* 293–304.

Shen, J., Sulkowski, J., Beckner, M., & Dailly, A. (2015). Effects of textural and surface characteristics of metal-organic frameworks on the methane adsorption for natural gas vehicular application. *Microporous and Mesoporous Materials, 212,* 80–90.

Sun, W., Feng, Y., Jiang, C., & Chu, W. (2015). Fractal characterization and methane adsorption features of coal particles taken from shallow and deep coalmine layers. *Fuel, 155,* 7–13.

Thommes, M. (2010). Physical adsorption characterization of nanoporous materials. *Chemie Ingenieur Technik, 82*(7), 1059–1073.

Walker, P. L., & Mahajan, O. P. (1993). Pore structure in coals. *Energy & Fuels, 7*(4), 559–560.

Wang, Y., Zhu, Y., Liu, S., & Zhang, R. (2016). Pore characterization and its impact on methane adsorption capacity for organic-rich marine shales. *Fuel, 181,* 227–237.

Xu, S., Han, Z., Wu, R., Cheng, J., & Xu, G. (2018a). Correlating micro/meso pore evolution and chemical structure variation in a mild thermal treatment of a subbituminite. *RSC Advances, 8*(18), 9754–9761.

Xu, S., Lai, D., Zeng, X., Zhang, L., Han, Z., Cheng, J., et al. (2018b). Pyrolysis characteristics of waste tire particles in fixed-bed reactor with internals. *Carbon Resources Conversion, 1*(3), 228–237.

Xu, G., Yang, Y.-P., Lu, S.-Y., Li, L., & Song, X. (2011). Comprehensive evaluation of coal-fired power plants based on grey relational analysis and analytic hierarchy process. *Energy Policy, 39*(5), 2343–2351.

Xu, S., Zeng, X., Han, Z., Cheng, J., Wu, R., Chen, Z., et al. (2019). Quick pyrolysis of a massive coal sample via rapid infrared heating. *Applied Energy, 242,* 732–740.

Yang, R. T., & Saunders, J. T. (1985). Adsorption of gases on coals and heat treated coals at elevated temperature and pressure. *Fuel, 64*(5), 616–620.

Yao, Y., Liu, D., Tang, D., Tang, S., & Huang, W. (2008). Fractal characterization of adsorption-pores of coals from North China: An investigation on CH_4 adsorption capacity of coals. *International Journal of Coal Geology, 73*(1), 27–42.

Yao, Y., Liu, D., & Xie, S. (2014). Quantitative characterization of methane adsorption on coal using a low-field NMR

relaxation method. *International Journal of Coal Geology, 131,* 32–40.

Zhang, Y., Lebedev, M., Smith, G., Jing, Y., Busch, A., & Iglauer, S. (2019a). Nano-mechanical properties and pore-scale characterization of different rank coals. *Natural Resources Research, 29*(3), 1787–1800.

Zhang, K., Wang, L., Cheng, Y., Li, W., Kan, J., Tu, Q., et al. (2019b). Geological control of fold structure on gas occurrence and its implication for coalbed gas outburst: case study in the qinan coal mine, huaibei coalfield. *China. Natural Resources Research, 29*(2), 1375–1395.

Zhao, Y., Liu, S., Elsworth, D., Jiang, Y., & Zhu, J. (2014). Pore structure characterization of coal by synchrotron small-angle X-ray scattering and transmission electron microscopy. *Energy & Fuels, 28*(6), 3704–3711.

Zuo, W. E. J., Liu, X., Peng, Q., Deng, Y., & Zhu, H. (2016). Orthogonal experimental design and fuzzy grey relational analysis for emitter efficiency of the micro-cylindrical combustor with a step. *Applied Thermal Engineering, 103,* 945–951.